A note on the Cahn solute drag model

Aulia Tegar Wicaksono

Department of Materials Engineering, The University of British Columbia

tegar@alumni.ubc.ca

Written on: July 22, 2015

Abstract

This document is a note on the Cahn solute drag model based on recent work in the literature. The solute drag models, in general, predict the magnitude of retardation of grain boundary migration due to solute segregation. An overview of classical solute drag model by Cahn is first presented. This is followed by some notes on the model, including a modified phenomenological model proposed by the author and a discussion on the solute drag model for the case of solutes with inhibited diffusion at the boundary.

1 Formalism of the Cahn model

Initially proposed by Lücke-Detert [1], revised by Cahn [2], Lücke-Stüwe [3] and later extended by Hillert [4, 5], solute drag models predict the drag effect during the steady-state migration of a grain boundary. These models share a number of similarities; Cahn's version will be used as an illustration for its simplicity.

During their interaction with a moving boundary, solute atoms maintain a concentration profile $C(z)$, where z is the distance from the grain boundary plane, that depends on the solute diffusivity profile $D(z)$, the binding energy profile $E_b(z)$ and the boundary velocity V. At steady state, the concentration profile can be obtained by first assuming a reasonable profile of $D(z)$ and $E_b(z)$, e.g. Figure 1 (a), and then solving the following

second-order linear diffusion equation, [2]

$$C'' + \left(E_b' + \frac{D'}{D} + \frac{V}{D} \right) C' + \left(\frac{D'}{D} E_b' + E_b'' \right) C = 0 \tag{1}$$

where $[']$ is a differential operator with respect to z. The drag-pressure P_d is the sum of force exerted by each solute atom on the boundary, [2]

$$P_d = -\frac{1}{\Omega} \int_{-\infty}^{+\infty} \left[C(z) - C_0 \right] E_b' dz \tag{2}$$

where Ω is the bulk atomic volume and C_0 is the bulk concentration.

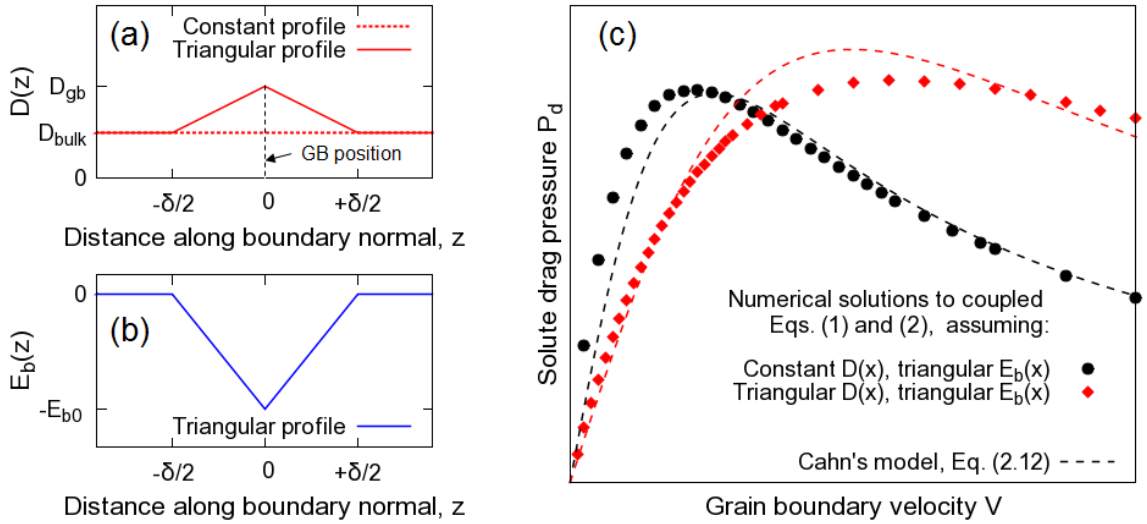

Fig. 1: Examples of (a) diffusivity profiles $D(z)$ and (b) binding energy profile $E_b(z)$, δ and E_{b0} being the grain boundary width and the maximum binding energy, respectively, (c) solute drag pressure dependence on boundary velocity; data points are the solutions to Eqs. (1) and (2) while the dashed lines are the model from Eq. (3).

While the coupled Eqs. (1) and (2) can be solved analytically in the limit of low or high velocity, a closed form expression for the drag pressure is not available. To approximately merge responses obtained in the high and low velocity limit, Cahn proposed the following expression [2],

$$P_d = \frac{\alpha C_0 V}{1 + (\beta V)^2} \tag{3}$$

where the parameters α and β depend on $D(z)$ and $E_b(z)$ via [2]

$$\alpha = \frac{4k_BT}{\Omega}\int_{-\infty}^{+\infty}\frac{\sinh^2\left[E_b(z)/2k_BT\right]}{D(z)}dz \tag{4}$$

$$\beta^2 = \frac{\alpha k_BT}{\Omega}\left[\int_{-\infty}^{+\infty}\left[E_b'(z)\right]^2 D(z)dz\right]^{-1} \tag{5}$$

Comparisons between the model in Eq. (3) and a numerical solution to the coupled Eqs. (1) and (2) are shown in Figure 1(c). The poor fit quality of Eq. (3) is noted in the case where there is a change in solute diffusivity at the grain boundary, i.e. a triangular $D(x)$ profile, see Figure 1(a).

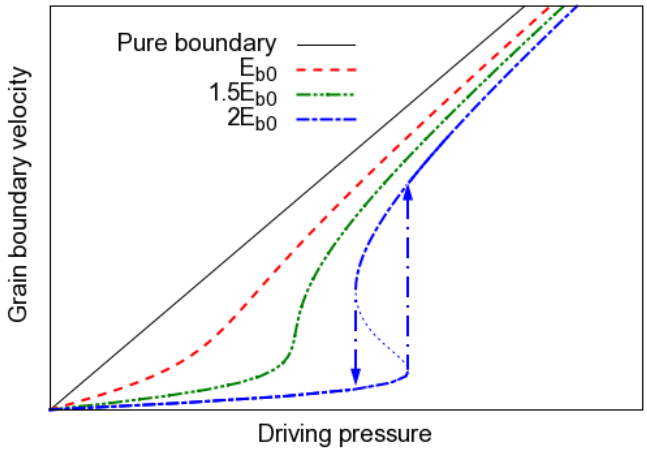

Fig. 2: The velocity-driving pressure relationship predicted by the Cahn solute drag model under different binding energies. The curve labelled '$2E_{b0}$' illustrates a hysteresis denoting different paths for abrupt break-away transitions, the dotted part representing the so-called unstable regime.

In regard to grain boundary migration, solute drag models postulate that the driving pressure P is dissipated via the intrinsic migration of the boundary, P_{int}, and the transport of segregated solute atoms along with the boundary as the boundary migrates, P_d, i.e. [2]

$$P = P_{\text{int}} + P_d \tag{6}$$

where P_{int} is given by the ratio of grain boundary velocity V and intrinsic mobility M, while P_d is given by Eq. (3). The solute drag component P_d reduces the energy available to drive the boundary, thus resulting in a low mobility when the driving pressure is small. If the driving pressure continues to increase, the boundary may gradually escape from the solute cloud, causing the migration to transition from a solute-loaded state (low

mobility) to a solute-free state (high mobility), see Figure 2. Such a transition can also occur in the opposite direction, i.e. the case where the driving pressure is initially large (the high mobility regime) and progressively decreasing. Depending on the interaction parameters, the transition may take place abruptly and the driving pressure where the transition occurs may depend on the direction at which the driving pressure changes, i.e. from low P to high P, and vice versa, see Figure 2.

The Cahn model has been revisited on several occasions. Lücke-Stüwe [3] provided a correction to account for site-saturation, leading to a segregation that is consistent with the Langmuir-McLean model [6]. Hillert generalized the model by substituting the binding energy profile with the chemical potential gradient profile [5], extending the model's compatibility to the case of heterophase interface in a multicomponent system. An interesting consequence of the Hillert model is that solute atoms at the interphase may act as a driving force (as opposed to a retarding force) for the interphase migration during phase transformations.

Many studies have implemented solute drag models to rationalize experimental results on solute-boundary migration. The Cahn model, for example, was used in the study of Nb effect on the recrystallization and grain-growth of α-Fe, enabling the estimation of parameters such as the binding energy of Nb to α-Fe grain boundaries and trans-interface diffusivity of Nb [7]. In another study, the Cahn model was used to identify the optimal Mn content in a low-carbon high-Nb steel to retard the kinetics of static recrystallization [8], thereby allowing steels to achieve a final grain-size of less than 3 μm [9].

While experimental observations seem to align with solute drag models, several predictions have yet to be experimentally verified. For example, the model predicts that the drag effect of solute with an attractive binding energy will be equal to that of solute with repulsive binding energy. Designing experiments to verify such an effect may be challenging as parameters that are relevant may not be accessible or easily tuned.

2 Recent work on solute drag problems

2.1 Background

A recent study by the present author investigated the interaction between a migrating grain boundary and diffusing solute atoms via kinetic Monte Carlo [10]. The Cahn original model was unable to provide an adequate fit to simulation results presented in that study. A modified model was proposed. Additionally, a sensitivity analysis of the model was performed in which two cases are considered: solutes that diffuse faster at the bound-

ary and solutes that diffuse slower at the boundary. The model produces a prediction that may be deemed counterintuitive: the drag pressure of an enriched boundary is much smaller than the drag pressure of a depleted boundary.

2.2 Modified solute drag model

In the Cahn original model, Eq. (3), the task of determining the parameters (α, β), given a data set of P_d versus V, is completed by performing a linear regression of V^2 versus V/P_d. The slope b and the ordinate intercept $-k$ of such regression are related to the model parameters via $\alpha = [(b/k)]/C_0$ and $\beta = 1/\sqrt{k}$.

It was found that such a procedure was unable to provide an adequate fit to simulation results presented in as well as in another study that employed phase-field crystals [11]. Such an inadequacy is originated from the fact that the regression form of the Cahn model showed a parabolic instead of linear trend. The following model is proposed,

$$P_d = \frac{\alpha C_0 V}{(1+\beta V)^2} \tag{7}$$

where parameters (α, β) are model parameters. The regression form of the modified model (Eq. (7)), i.e. V versus $\sqrt{V/P_d}$, produces a linear trend. Parameters of the modified model have the same units as the original model. They are related to the slope b and the ordinate intercept $-k$ of the regression via $\alpha = [(b/k)^2]/C_0$ and $\beta = 1/k$.

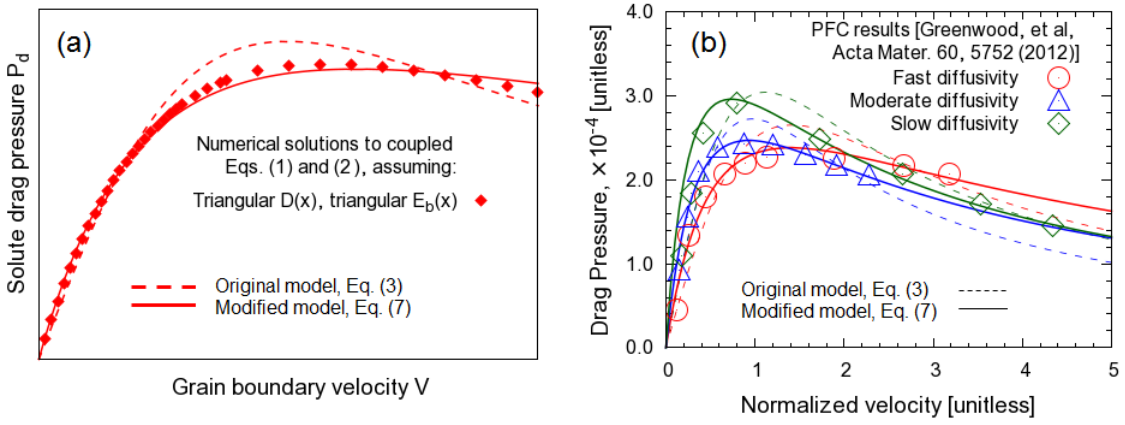

Fig. 3: (a) The drag pressure data from Figure 1(c), now being fit to the modified solute drag model. (b) The PFC simulation results from the literature [11] on the drag pressure variation with velocity for different solute diffusivities, being fit to both the original and the modified solute drag models.

The modified model has also been implemented in other applications. Figure 3(a) and

(b) show the application of the modified model to fit the numerical solution of solute-drag diffusion equation (see Figure 1(c)) and the results from other atomistic simulations, i.e. the phase-field crystals method presented in [11], respectively. The close alignment between the modified model and the data set, as demonstrated in these figures, suggest that the modified model provides a better description of the solute drag dependence on the boundary velocity than the original model.

A further potential application of the modified model is related to the development of models on complex microstructural evolution, e.g. via classical phase field techniques [12]. In these models, the effect of impurities on the kinetics of boundary migration is considered by implementing continuum expressions such as the solute drag model by Cahn, i.e. Eq. (3), or the particle pinning model by Zener [13]. These expressions are used to estimate the local drag pressure of a boundary segment migrating at a certain velocity due to its local curvature [12]. Microstructural features predicted by these models, e.g. the average grain size, are thus dependent upon the type of impurity drag expressions being assumed.

2.3 Diffusivity at the grain boundary

It is a view commonly subscribed by classical literature that solute atoms have a higher diffusivity in the grain boundary than they do in the matrix [14, 15]. The enhancement of diffusivity at the boundary is rationalized in terms of grain boundary free volume, which is argued as a fast diffusion path for segregated solute atom [14]. The universality of such concept has been recently put into question in a number of study.

A recent work by Teus et al [16] investigates the diffusion of carbon and cobalt in ferrite grain boundaries from experiments. Using sectioning method and radiography, they concluded that the diffusivity enhancement is observed for cobalt, a substitutional element in ferrite matrix. The carbon diffusivity at ferrite grain boundaries, however, is lower than the bulk diffusivity of carbon. A similar trend in the inhibition of interstitial solute diffusion at the boundary has also been reported in other study, e.g. helium in ferrite [17, 18], helium in tungsten [19], hydrogen in ferrite [20, 21]. Furthermore, the inhibition of interstitial solute diffusion at the boundary has also been attributed to the formation of vacancy-solute complex at the boundary and the high dissociation energy associated with such complex [16, 18].

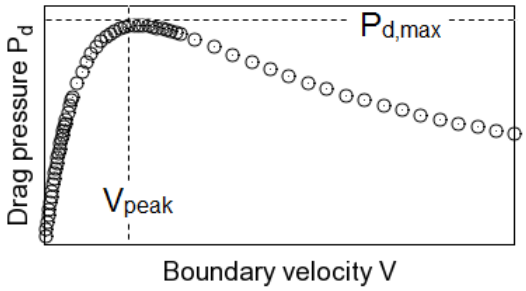

Fig. 4: A plot of drag pressure vs grain boundary velocity obtained from solving Eqs. (1) and (2) numerically. The maximum drag pressure $P_{d,\max}$ and the corresponding velocity (or peak velocity) V_{peak} are highlighted.

The effect of inhibited solute diffusion at the boundary on solute drag behaviour will now be assessed using the Cahn framework. Consider the triangular profiles of diffusivity and binding energy such as shown in Figure 1(a) and (b). The boundary diffusivity D_{gb} is assigned as the control variable while all other variables are kept constant, i.e. $C_0 = 0.01$, $E_{b0} = -2k_BT$, $D_{\text{bulk}} = 1$, $\delta = 2$, $\Omega = 1$, and units are all dimensionless. Eq. (1) is solved at a given velocity for $C(z)$, which is then substituted to Eq. (2) to obtain P_d. The resulting drag pressure is plotted as a function of velocity for a given D_{gb}, see Figure 4 for example. From this plot, the maximum drag pressure, $P_{d,\max}$, and the corresponding velocity, or peak velocity, V_{peak}, are extracted, see Figure 4.

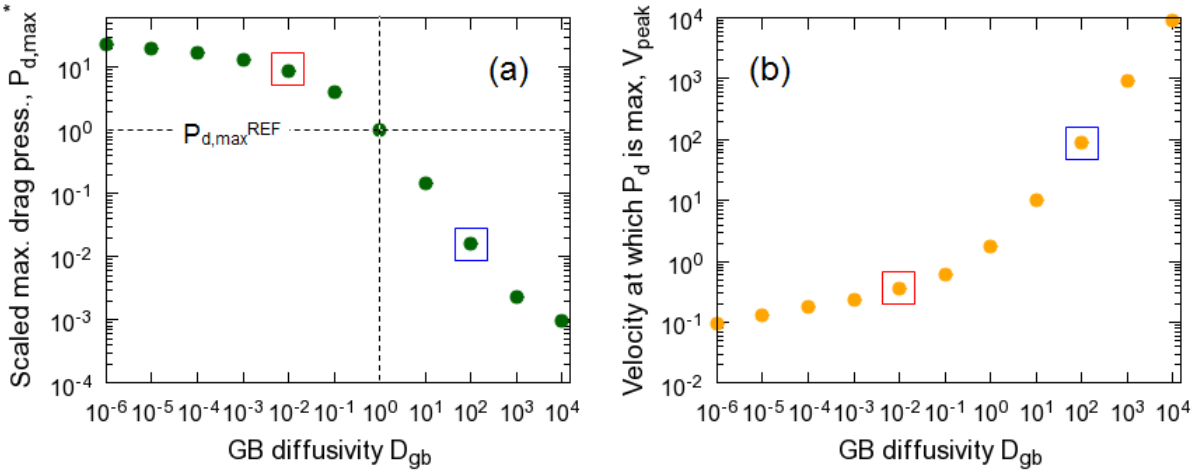

Fig. 5: Variation of (a) the scaled maximum drag pressure $P^*_{d,\max}$ and (b) the peak velocity V_{peak} with grain boundary diffusivity D_{gb}. The scaled maximum drag pressure $P^*_{d,\max}$ is the ratio between the maximum drag pressure for a given D_{gb} and the reference maximum drag pressure, i.e. $P^{\text{REF}}_{d,\max} = P_{d,\max}(D_{\text{gb}} = D_{\text{bulk}}{=}1)$.

The pairs ($P_{d,\max}$, V_{peak}) are obtained from a range of D_{gb} and plotted in Figure 5 (a) and (b), respectively. The maximum drag pressure in Figure 5(a) has been scaled by the reference maximum drag pressure, i.e. $P^{\text{REF}}_{d,\max} = P_{d,\max}(D_{\text{gb}} = 1)$. As indicated by Figure 5(a), solute atoms that are kinetically inhibited at the boundary impose a higher drag pressure than those that are kinetically enhanced at the boundary.

To explain such a trend, two cases will be analyzed in details, i.e. $D_{\text{gb}} = 10^2$ (enhanced diffusivity at the boundary) and $D_{\text{gb}} = 10^{-2}$ (inhibited diffusion at the boundary), see boxed data points in Figure 5(a) and (b). From Figure 5(b), the corresponding velocity at which the drag pressure is maximum are $V_{\text{peak}} = 0.35$ (for $D_{\text{gb}} = 10^{-2}$) and 90 (for $D_{\text{gb}} = 10^2$). Consider now the drag pressure dependence on the velocity in both cases, see Figure 6. It can be concluded, therefore, that for $V \leq 0.3$ (the left side of the vertical dashed line in Figure 6), the drag pressure in both data set (inhibited and enhanced) show a similar trend, i.e. that the drag pressure increases with increasing velocity.

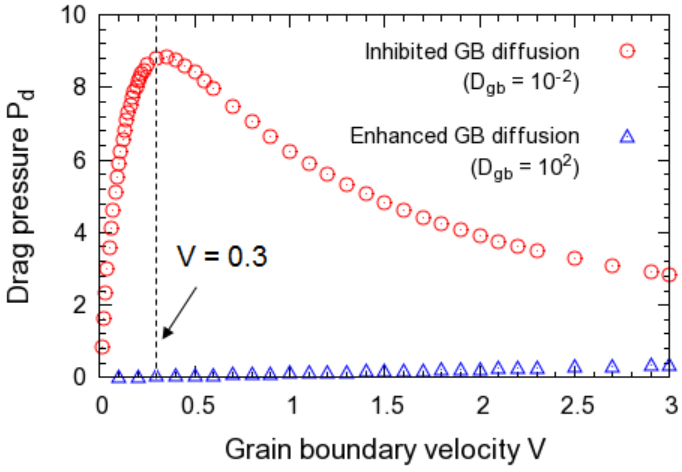

Fig. 6: The dependence of drag pressure on grain boundary velocity for two cases of solute diffusion: inhibited diffusion and enhanced diffusion at the boundary. For $V \leq 0.3$, P_d increases with increasing V.

Consider now the case where both boundaries migrate at the same velocity, i.e. $V = 0.2$. This velocity lies on the regime where P_d increases with increasing, i.e. the left side of dashed vertical line in Figure 6. At this velocity, the drag pressure is $P_d = 9$ (for $D_{\text{gb}} = 10^{-2}$) and 0.01 (for $D_{\text{gb}} = 10^2$), while the corresponding concentration profiles at steady state are presented in Figure 7(a) and (b), respectively. Both profiles are asymmetric but to a different extent. They also demonstrate regimes of solute enrichment and depletion at the boundary. The net segregation for the case of enhanced boundary diffusion (Figure 7(b)) is much larger than the net segregation for the case of inhibited boundary diffusion

(Figure 7(a)). The contrast in the net segregation for both cases is particularly interesting when correlated with the contrast in the drag pressure: *in order to drive a solute-enriched boundary at the same velocity as a solute-depleted boundary, the portion of driving pressure being dissipated due to transporting segregating solute (i.e. the solute drag pressure) is less in the former than it is in the latter case.*

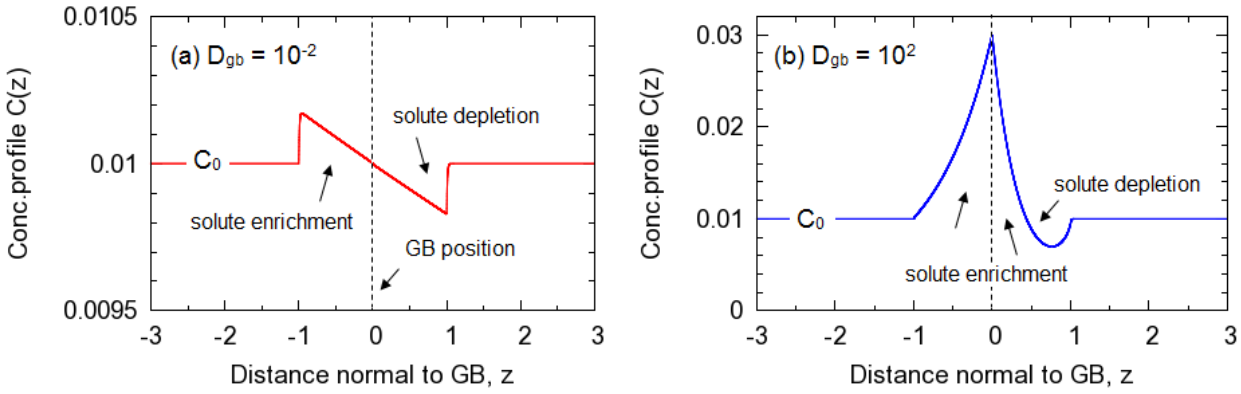

Fig. 7: The concentration profile at steady state for (a) inhibited solute diffusion at the boundary, and (b) enhanced solute diffusion at the boundary.

It is fair to say that the implication printed in italic above is counterintuitive, at least to the author[1]. Such an implication is a mathematical (not physical) consequence of the model assumption where the sign of gradient binding energy profile determines the drag pressure magnitude. For the triangular binding energy profile shown in Figure 1(b), the gradient on the left side of boundary is negative ($E_b'(z) = -2|E_{b0}|/\delta$ for $-\delta/2 \leq z < 0$) while that on the right side is positive, ($E_b'(z) = 2|E_{b0}|/\delta$ for $0 < z \leq \delta/2$). It is worth to recall that the model postulates the drag pressure as proportional to the product of net segregation (i.e. $C(z) - C_0$) and gradient of binding energy (i.e. $E_b'(z)$), see Eq. (2). For the case of enhanced boundary diffusion, the term $[C(z) - C_0] \times E_b'(z)$ on the left side of the boundary is similar in magnitude but opposite in sign to the term $[C(z) - C_0] \times E_b'(z)$ on the right side of the boundary. On the other hand, for the case of inhibited boundary diffusion, the term $[C(z) - C_0] \times E_b'(z)$ on the left and the right side of the boundary are not only similar in magnitude but also equal in sign. Since the net drag pressure is the sum of contribution from both sides of the boundary,

[1] An equivalent analogy to describe the counterintuition of such conclusion is to say that a 5-seated car that carries 4 people (1 driver and 3 passengers at the back row) burns less gas than the same type of car carrying 1 drive and 1 passenger at the back row does, both cars moving at the same speed.

the drag pressure in the case of enhanced boundary diffusion will be much less than that in the case of inhibited boundary diffusion, despite the net segregation being much higher in the former than in the latter case.

This particular topic was presented by the author in a symposium discussion in the 2015 ALEMI (www.alemi.ca) meeting, which was held in conjunction with the PTM conference in Whistler, B.C (www.ptm2015.org). It was suggested by a participant of the discussion that the statement printed in bold in a box above is not surprising, though indeed counterintuitive, since the drag pressure should be understood as an effect not only due to the amount of segregated solute but also to the extent of asymmetry in the concentration profile of segregated solute. While such an explanation may be feasible, it is not consistent with what the model actually predicts. For example, both profiles in Figure 7(a) and (b) are asymmetric but to a different extent. It would be unsound to argue that Figure 7(a) is more asymmetric than Figure 7(b). Presently, the author offers no alternative explanation, much less a mathematical model, that can resolve this issue. After all, this letter is aimed to highlight some inconsistencies associated with the classical solute drag model, which only came to attention recently because an increasing number of study has employed atomistic simulations to investigate the solute drag problems.

3 Computer codes for solving the solute drag model

A script in C language for obtaining the solution to Eqs. (1) and (2) has been written and available online [22]. At this moment, the script is capable of constructing a triangular profile of both diffusivity and binding energy, see Figure 1(a) and (b), by setting the parameters D_{bulk}, D_{gb} and E_{b0}. Uniform profiles can be constructed by setting $D_{\text{bulk}} = D_{\text{gb}}$.

References

[1] K. Lücke, K. Detert, *A quantitative theory of grain-boundary motion and recrystallization in metals in the presence of impurities*. Acta Metall. **5**, 628 (1957). doi:10.1016/0001-6160(57)90109-8

[2] J.W. Cahn, *The impurity-drag effect in grain boundary motion*. Acta Metall. **10**, 789 (1962). doi:10.1016/0001-6160(62)90092-5

[3] K. Lücke, H. Stüwe, *On the theory of impurity controlled grain boundary motion*. Acta Metall. **19**, 1087 (1971). doi:10.1016/0001-6160(71)90041-1

[4] M. Hillert, B. Sundman, *A treatment of the solute drag on moving grain boundaries and phase interfaces in binary alloys*. Acta Metall. **24**, 731 (1976). doi:10.1016/0001-6160(76)90108-5

[5] M. Hillert, *Solute drag in grain boundary migration and phase transformations*. Acta Mater. **52**, 5289 (2004). doi:10.1016/j.actamat.2004.07.032

[6] D. McLean, *Grain Boundaries in Metals* (Clarendon Press, 1957)

[7] C.W. Sinclair, C.R. Hutchinson, Y. Bréchet, *The effect of Nb on the recrystallization and grain growth of ultra-high-purity α-Fe: a combinatorial approach*. Metall. Mater. Trans. A **38**, 821 (2007). doi:10.1007/s11661-007-9106-9

[8] H.S. Zurob, G. Zhu, S.V. Subramanian, G.R. Purdy, C.R. Hutchinson, Y. Bréchet, *Analysis of the effect of Mn on the recrystallization kinetics of high Nb steel: an example of physically-based alloy design*. ISIJ International **45**, 713 (2005). doi:10.2355/isijinternational.45.713

[9] A.J. DeArdo, *Niobium in modern steels*. Int. Mater. Rev. **48**, 371 (2003). doi:10.1179/095066003225008833

[10] A.T. Wicaksono, C.W. Sinclair, M. Militzer, *A three-dimensional atomistic kinetic Monte Carlo study of dynamic solute-interface interaction*. Modell. Simul. Mater. Sci. Eng. **21**, 085010 (2013). doi:10.1088/0965-0393/21/8/085010. URL `http://arxiv.org/abs/1306.2884`

[11] M. Greenwood, C. Sinclair, M. Militzer, *Phase field crystal model of solute drag*. Acta Mater. **60**, 5752 (2012). doi:10.1016/j.actamat.2012.06.056

[12] S. Shahandeh, M. Greenwood, M. Militzer, *Friction pressure method for simulating solute drag and particle pinning in a multiphase-field model*. Modell. Simul. Mater. Sci. Eng. **20**, 065008 (2012). doi:10.1088/0965-0393/20/6/065008

[13] C.S. Smith, *Grains, Phases and Interfaces: An interpretation of microstructure*. Trans. AIME **175**, 15 (1949)

[14] D.A. Porter, K.E. Easterling, *Phase Transformations in Metals and Alloys* (CRC Press, 1992)

[15] G. Gottstein, L. Shvindlerman, *Grain Boundary Migration in Metals* (CRC Press, 2010). doi:10.1201/9781420054361

[16] S.M. Teus, V.F. Mazanko, J.M. Olive, V.G. Gavrilijuk, *Grain boundary migration of substitutional and interstitial atoms in α-iron*. Acta Mater **69**, 105 (2014). doi:10.1016/j.actamat.2014.01.049

[17] A.T. Wicaksono, M. Militzer, C.W. Sinclair, *Atomistic simulations of the effect of helium clusters on grain boundary mobility in iron*. IOP Conf. Series: Materials Science and Eng. **88** (2015)

[18] H.Q. Deng, W.Y. Hu, F. Gao, H.L. Heinisch, S.Y. Hu, Y.L. Li, R.J. Kurtz, *Diffusion of small He clusters in bulk and grain boundaries in α-Fe*. J. Nucl. Mater. **442**, S667 (2013). doi:10.1016/j.jnucmat.2013.02.063

[19] K.D. Hammond, L. Hu, D. Maroudas, B.D. Wirth, *Helium impurity transport on grain boundaries: Enhanced or inhibited?* Europhys. Lett. **110**, 52002 (2015). doi:10.1209/0295-5075/110/52002

[20] J. von Pezold, L. Lymperakis, J. Neugebauer, *Hydrogen-enhanced local plasticity at dilute bulk H concentrations: The role of H-H interactions and the formation of local hydrides*. Acta Mater **59**, 2969 (2015). doi:10.1016/j.actamat.2011.01.037

[21] X. Liu, W. Xie, W. Chen, H. Zhang, *Effects of grain boundary and boundary inclination on hydrogen diffusion in α-iron*. J. Mater. Res. **26**, 2735 (2011). doi:10.1557/jmr.2011.262

[22] *tegarwicaksono/solutedrag (github repository)*. doi:10.5281/zenodo.20977